Composition-Dependent Apparent Activation-Energy and Sluggish Grain-Growth in High Entropy Alloys

B. Gwalani – University of North Texas
R. Salloom – University of North Texas
T. Alam – University of North Texas
S. G. Valentin – University of North Texas
X. Zhou – University of Alabama
G. Thompson – University of Alabama
S. G. Srinivasan – University of North Texas
R. Banerjee – University of North Texas

Citation of published version:
Gwalani, B., Salloom, R., Alam, T., Valentin, S., Zhou, X., Thompson, G., Srinivasan, S., Banerjee, R. (2019): Composition-Dependent Apparent Activation-Energy and Sluggish Grain-Growth in High Entropy Alloys. *Materials Research Letters*. 7(7).

DOI: https://doi.org/10.1080/21663831.2019.1601644

MATER. RES. LETT.
2019, VOL. 7, NO. 7, 267–274
https://doi.org/10.1080/21663831.2019.1601644

MATERIALS RESEARCH LETTERS
Taylor & Francis
Taylor & Francis Group

ORIGINAL REPORT

Composition-dependent apparent activation-energy and sluggish grain-growth in high entropy alloys

B. Gwalani[a,b]*, R. Salloom[a], T. Alam[a], S. G. Valentin[a], X. Zhou[c], G. Thompson[c], S. G. Srinivasan[a] and R. Banerjee[a,b]

[a]Department of Materials Science and Engineering, University of North Texas, Denton, TX, USA; [b]Advanced Materials and Manufacturing Processes Institute, University of North Texas, Denton, TX, USA; [c]Department of Metallurgical and Materials Engineering, The University of Alabama, Tuscaloosa, AL, USA

ABSTRACT

Experimental results reveal that the apparent activation-energy for grain-growth in an *fcc*-based $Al_xCoCrFeNi$ high entropy alloy (HEA) system increases from 179 to 486 kJ/mol when the Al content increases from $x = 0.1$ to 0.3. These unexpectedly high apparent activation-energy values can be potentially attributed to solute clustering within the *fcc* solid-solution phase that develops with increasing Al content in this HEA. Detailed microstructural analysis using atom-probe tomography and density functional theory (DFT) calculations strongly indicate the presence of such nanoscale clusters. This phenomenon can change grain-growth from a classical solute-drag regime to a much more sluggish cluster-drag based mechanism in these HEAs.

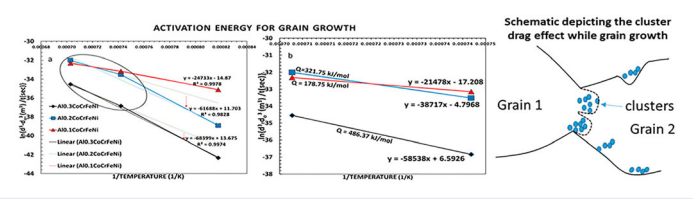

ARTICLE HISTORY
Received 5 November 2018

KEYWORDS
High entropy alloy; grain-growth; activation-energy; atom-Probe tomography

IMPACT STATEMENT

First report on a composition dependent change in apparent activation-energy for grain-growth in high entropy alloys. A novel cluster drag effect inhibiting grain-growth kinetics is suggested.

Traditionally alloy development has been largely based on choosing a single major element called the principal element and adding minor elements to develop the best balance of properties. For instance, Cr, Ni, and Mo are added in small proportions into steels, to enhance various physical and chemical properties. The more recent development of high entropy alloys (HEAs), brought about a paradigm shift by including five or more elements mixed in equiatomic or near-equiatomic ratios. Despite the inherent compositional complexity of these alloys, their final microstructures are often similar to conventional alloys, either consisting of a single disordered random solid solution phase or a mixture of ordered phases or disordered solid solution phases [1]. Considering the highly complex concentrated solid solution nature of HEAs, developing a fundamental mechanistic understanding of diffusion and kinetics is essential and could potentially reveal mechanisms that are typically unseen in solvent-rich and solute-lean systems conventional metallic alloys. Recent neutron diffraction experiments of Ma et al. [2] conclusively showed the presence of Al-rich short-range ordered domains in *fcc*-based single-phase HEA alloy. These nano-domains can influence the grain-growth, dislocation-movement, amenability for deformation-twinning, friction-coefficient, Hall-Petch coefficient, etc. all of which can, in turn, affect the overall performance of the material.

The strength, toughness or formability of most polycrystalline single-phase materials strongly depends on the average grain size, the size distribution and the nature of the grain boundaries. Thus, understanding the kinetics of grain-growth and grain-boundary migration

CONTACT R. Banerjee raj.banerjee@unt.edu Department of Materials Science and Engineering, University of North Texas, Denton, TX 76207, USA; Advanced Materials and Manufacturing Processes Institute, University of North Texas, Denton, TX 76207, USA
*Present address: Physical and Computational Sciences Directorate, Pacific Northwest National Laboratory, 902 Battelle Blvd, Richland, WA, USA.

Supplemental data for this article can be accessed here. https://doi.org/10.1080/21663831.2019.1601644

in HEAs becomes even more interesting and intriguing due to the added complexity of the concentrated solid solution nature and the absence of any obvious single principal alloying element. The various factors that can influence grain-boundary motion are stored deformation energy (~ 10 MPa), grain-boundary energy ($\sim 10^{-2}$ MPa), surface energy ($\sim 10^{-4}$ MPa), chemical driving force ($\sim 10^{2}$ MPa), magnetic driving force ($\sim 10^{-4}$ MPa), elastic energy ($\sim 10^{-4}$ MPa), and temperature gradient ($\sim 10^{-5}$ MPa) [3].

Typically, the free energy of the system is reduced by grain-growth via boundary migration, resulting in a reduction in the total boundary area. The motion of grain boundaries involves 'short-range' jumps of atoms or ions across the grain boundary to align with the crystallographic orientation of the growing grain.

Typically, driving force for classical grain-growth in elemental materials is the boundary curvature determined by the internal pressure difference

$$\Delta P = \frac{\alpha.\gamma_{GB}}{G}$$

ΔP is the difference in pressure between adjacent grains, α is the geometric factor, γ_{GB} is the grain-boundary energy, G is the grain size.

The kinetics of classical grain-growth is often quantified by analyzing grain-size as a function of isothermal annealing time for different temperatures [3–6]. The local velocity of the grain boundary at any point is proportional to the local curvature and elastic strain effects are ignored.

For a given temperature, the grain diameter grows parabolically with time as:

$$d^2 - d_o^2 = kt \tag{1}$$

where d is the instantaneous grain size; d_o is the initial grain-size; t is time; and k is a kinetic constant that depends on the temperature and grain-boundary energy.

Equation (1) has often been generalized for solute-containing systems, as:

$$d^n - d_o^n = kt \tag{2}$$

The value of n, varies from 2 to 7, determines the growth mechanism and k defines the diffusion processes [5–7]. Grain-growth in a number of carbon steels between 815°C and 1250°C have been studied and reported values for n ranging between 3 and 7 [3]. The deviation in the value of n from 2 was attributed by Grey and Higgins [8,9] to the clustered atoms inhibiting grain-growth because grain-boundary motion would now require these clusters rather than simply single atoms (classical solute-drag model) to be mobile. Additionally, small amounts of impurities have been shown to reduce grain boundary velocity by over an order of magnitude, which have been attributed to impurity atoms pinning grain boundaries and retarding their motion [7–16]. Furthermore, small particles of a second phase provide one of the most effective drag force in grain-boundary migration. The drag by particles on a moving grain boundary is usually considered in the Zener approximation, where the particles act as a stationary pinning center for the boundaries [14,15]. However, it is well known that inclusions in solids are not immobile and that particle mobility increases drastically with decreasing particle size. Therefore, small particles can move along with the boundary and severely constrain grain-boundary migration. Here, we analyze the influence of different levels of Al addition on grain-growth kinetics in an equiatomic quaternary alloy (CoCrFeNi), complementing experiments and DFT calculations. Based on the results of the grain-growth kinetics, the apparent activation-energy for grain-growth has been determined, as a function of Al content in these fcc Al_xCoCrFeNi alloys. The results have been rationalized based on a possible cluster-drag based mechanism of grain-growth, eventually leading to the well-known Zener-pinning model, when second phase precipitates are formed at the fcc grain boundaries. A novel cluster drag phenomenon is suggested as the Al concentration increases.

Alloys with nominal chemical composition $Al_{0.1}$CoCrFeNi, $Al_{0.2}$CoCrFeNi and $Al_{0.3}$CoCrFeNi were prepared by conventional arc melting, and microstructural characterization was performed using scanning electron microscopy (FEI Nova-NanoSEM 230™) and atom-probe tomography (in Cameca Local Electrode Atom-Probe (LEAP) 3000X HR and 5000XS) 3D atom-probe. The atom-probe tips were prepared on FEI Nova 200 dual beam focused ion beam [17]. The arc melting chamber containing the raw materials was evacuated to $\sim 10^{-3}$ Pa, flushed twice with pure Ar, and finally backfilled with Ar to a pressure of $\sim 5 \times 10^4$ Pa. The buttons were flipped and re-melted five times to ensure chemical homogeneity before finally casting into a cylindrical copper mold. The cast ingots were sealed in evacuated quartz tubes, homogenized at 1200°C for 24 h followed by water quenching (WQ). After grinding and cleaning the surfaces, the homogenized ingots were cold rolled along their long axis to a reduction in thickness $\sim$90% and aged at 950°C, 1075°C and 1150°C for various times, followed by water quenching. The grain-size measurement was done using ImageJ software taking five SEM micrographs from each condition covering at least 100 grains from each sample. The grain-size measurement was calibrated with electron back scattered electron diffraction (EBSD) orientation microscopy. Grain-size distribution vs annealing

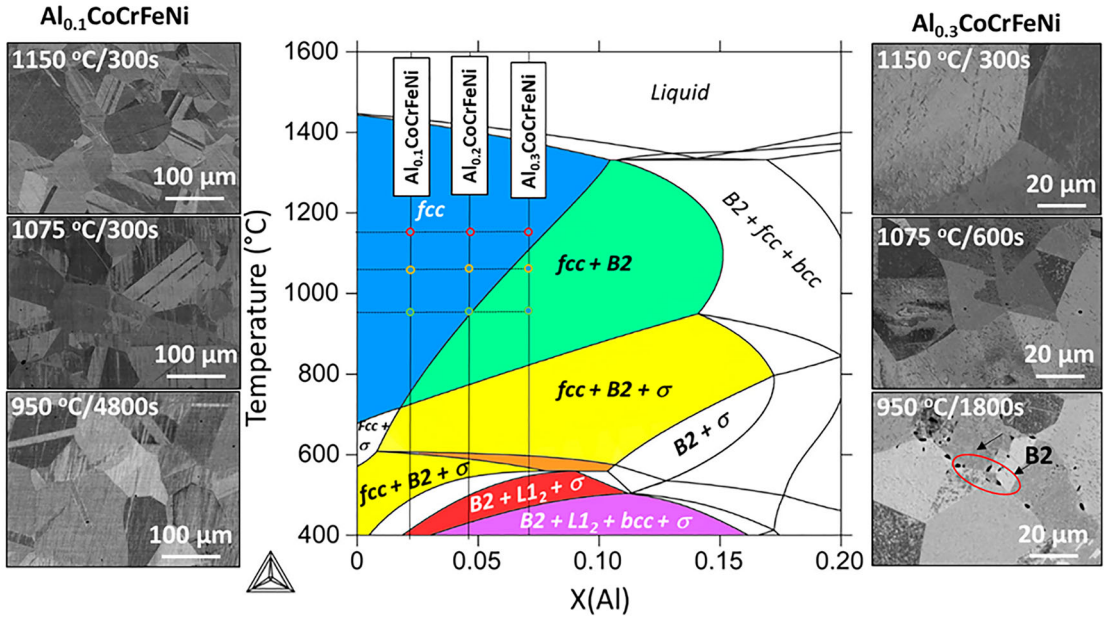

Figure 1. Isopleth for $Al_XCoCrFeNi$. It shows possible phases as a function of Al content and temperature. Left and Right side of the figure shows the SEM BSED images taken from $Al_{0.1}$CoCrFeNi and $Al_{0.3}$CoCrFeNi alloys respectively at 950°C, 1075°C and 1150°C.

temperature/time is shown in Supplementary Table 1 and Supplementary Figure S1.

The isopleth section with varying Al content for the Al_xCoCrFeNi system (Figure 1) is calculated using a computational-thermodynamic (CALPHAD approach) [18]. The composition $Al_{0.1}$CoCrFeNi, $Al_{0.2}$CoCrFeNi and $Al_{0.3}$CoCrFeNi are marked with vertical dotted lines on this isopleth, and the temperatures of 1150°C, 1075°C and 950°C are marked with a horizontal dotted line. While $Al_{0.1}$CoCrFeNi and $Al_{0.2}$CoCrFeNi alloys lie in the single *fcc* phase field in all three temperatures, the $Al_{0.3}$CoCrFeNi alloy has *fcc* + B2 phases as equilibrium phases at 1050°C and 950°C. After annealing at different temperatures, $Al_{0.1}$CoCrFeNi alloy shows completely recrystallized grains with no second phase precipitation (Figure 1, left side). However, second phase grain-boundary precipitates are clearly seen in $Al_{0.3}$CoCrFeNi alloy at 950°C (Figure 1, right-side). SEM-EBSD and TEM investigations conclude that these grain-boundary precipitates have B2 structure, as shown in Supplementary Figure S2.

The grain-growth data obtained from the $Al_{0.1}$, $Al_{0.2}$ and $Al_{0.3}$Cocrfeni HEAs were modeled using Equation (3). Regression analysis led to the best value of d_o and n that fits the $d^n - d_o^n$ vs t curve linearly at all three temperatures to be $d_o = 4.0$ and $n = 3.0$. Since the starting material is a cold-rolled plate, the grains start to recrystallize rather rapidly at the onset of annealing.

With $d_o = 4.0\,\mu m$ and $n = 3.0$, the grain-growth data at the three different temperatures (950°C/1223 K, 1075°C/1348 K and 1150°C/1423 K) as a function of annealing time are shown in Figure 2 for $Al_{0.1}$CoCrFeNi alloy. Similar plots for $Al_{0.2}$ and $Al_{0.3}$CoCrFeNi alloys are shown in Supplementary Figures S3–S4, respectively. The values of the kinetic-constants for grain-growth at the different temperatures (slope of the curve) have been determined and are tabulated in Supplementary Table 2. The activation-energy for grain-growth can be thus calculated from the kinetic constant values obtained at the three different temperatures, using Arrhenius' equation shown below:

$$k = Ae^{-E_a/(RT)} \tag{4}$$

where k is rate-constant for grain-growth and depends on absolute temperature T (in Kelvin), A is the pre-exponential factor, E_a is activation-energy, and R is universal gas constant.

Taking the natural-logarithm and rearranging the terms yields:

$$ln(k) = E_a/R(1/T) + ln(A) \tag{5}$$

The plots of $ln\ k$ vs $1/T$ for $Al_{0.1}$CoCrFeNi alloy is shown in Figure 2. Similar plots generated for $Al_{0.2}$CoCrFeNi and $Al_{0.3}$CoCrFeNi alloys are shown in Supplementary Figure S3 and S4. Note the sharp drop in the k value for $Al_{0.2}$CoCrFeNi and $Al_{0.3}$CoCrFeNi alloys at 950°C. Based on the thermodynamic predictions (and confirmed by SEM, EBSD, and TEM results) while the $Al_{0.1}$CoCrFeNi exhibits a single *fcc* phase at all annealing temperatures, the $Al_{0.2}$CoCrFeNi and $Al_{0.3}$CoCrFeNi alloys have a single stable *fcc* phase at 1075°C and 1150°C, but a two-phase *fcc* + B2 phase stability at 950°C.

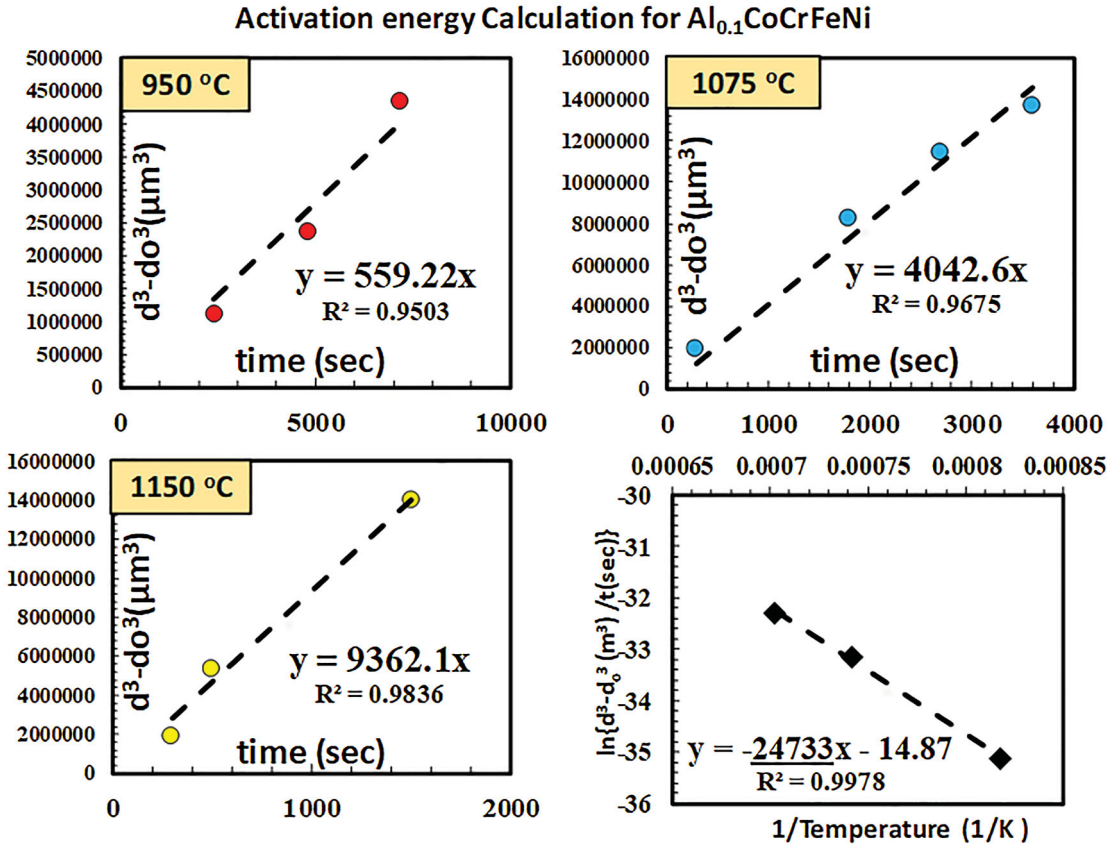

Figure 2. (a–c) plots showing grain diameter (d) raised to the power of three vs times (s) at 950°C, 1075°C and 1150°C for Al0.1CoCrFeNi (d) natural log of (k) is plotted with 1/T to calculate Ea.

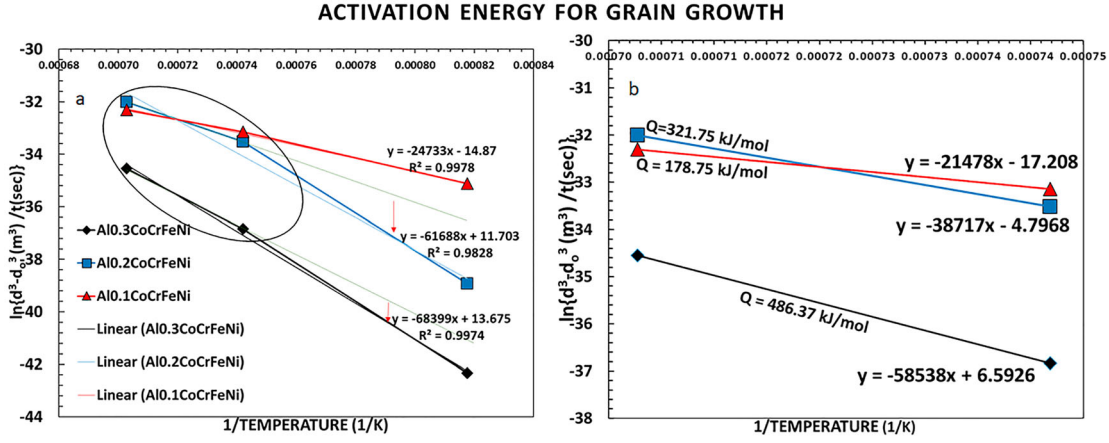

Figure 3. (a–b) Plots to calculate the activation-energy for grain-growth for $Al_{0.1}$, $Al_{0.2}$ and $Al_{0.3}$ CoCrFeNi HEAs.

Referring to Figure 3(a), it is apparent that while all three points, corresponding to the three temperatures, lie on the same straight line in case of the $Al_{0.1}$CoCrFeNi alloy, the situation is different in case of the $Al_{0.2}$CoCrFeNi and $Al_{0.3}$CoCrFeNi alloys. For these HEAs, containing higher amounts of Al, there is a distinct decrease in the slope between the latter two points (lower temperatures) as compared to the first two points, with the second point being a common one. Since the negative slope is directly proportional to the activation energy for grain growth, this difference is slope can be attributed to a change in activation energy resulting from a change in the grain growth mechanism at the lowest temperature (950°C) in case of $Al_{0.2}$CoCrFeNi and $Al_{0.3}$CoCrFeNi alloys. The precipitation of a second B2 phase on the grain boundaries at 950°C in case of these two alloys can change the grain-growth mechanism from a classical solute drag to a Zener-pinning like process. Hence, upon formation,

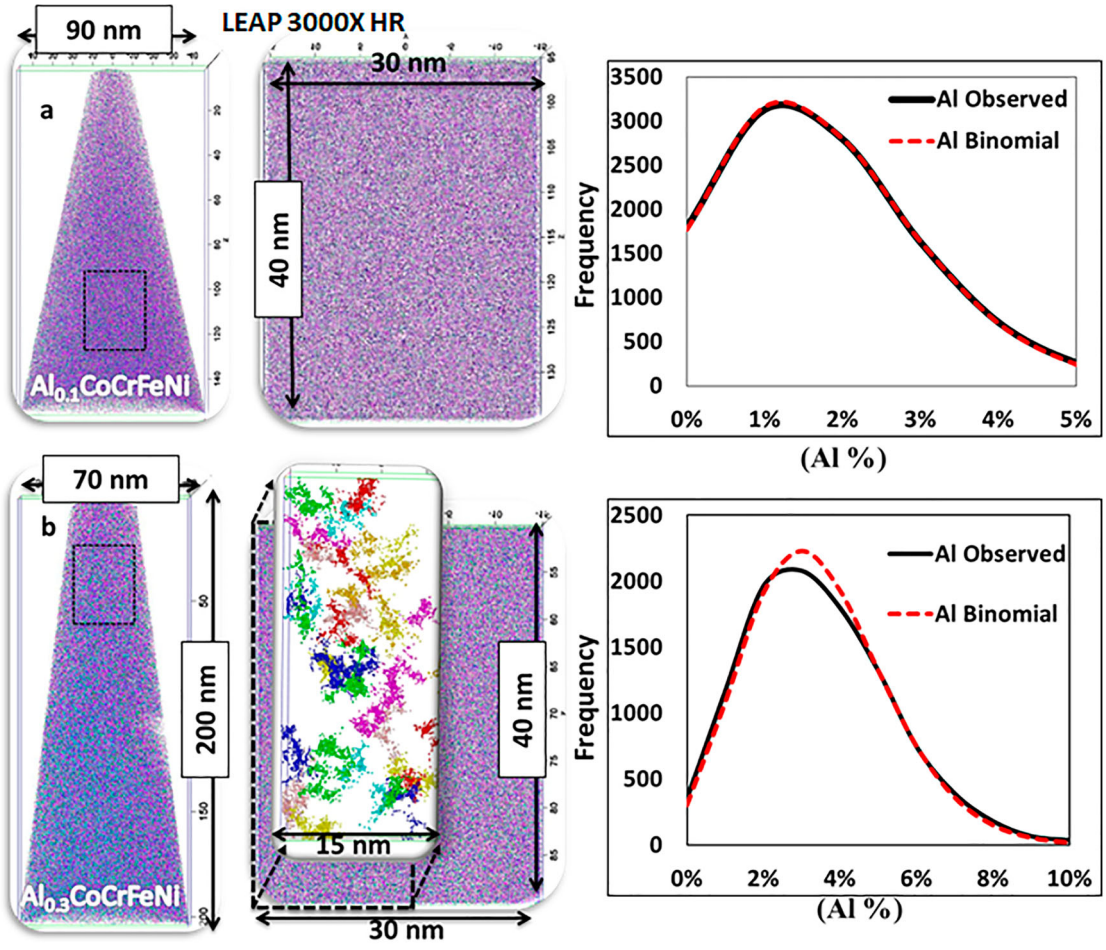

Figure 4. Atom-probe reconstruction (left), a magnified view of the highlighted region from the reconstruction (center) and binomial and observed distribution of Al atoms in the highlighted region (right) from (a) $Al_{0.1}$CoCrFeNi (b) $Al_{0.3}$CoCrFeNi.

B2 precipitates pin the grain boundaries and make the grain-growth extremely sluggish. Based on these experimental observations and restrictions imposed by the two-phase *fcc* + B2 mixture in case of the $Al_{0.2}$CoCrFeNi and $Al_{0.3}$CoCrFeNi alloys at 950°C, only the data from the two higher temperatures, 1150°C and 1075°C, have been used to calculate the apparent activation-energy for grain-growth for the three alloys, with all three exhibiting a stable single *fcc* phase based microstructure (Figure 3(b)).

The slope of the linear fit to the data multiplied by *R* (gas constant) gives the apparent activation-energy that was computed to be 178.75, 321.75 and 486.37 kJ/mol for $Al_{0.1}$, $Al_{0.2}$ and $Al_{0.3}$, respectively. The activation-energy of most single-phase metals is in the range of 50–700 kJ/mol [18]. There are only a few published reports of activation-energies for grain-growth in HEAs. Liu et al. reported a value of 327 kJ/mol for FeCrNi-CoMn [19], and Juan et al. reported a value of 389 kJ/mol for HfNbTaTiZr [20]. The high activation-energy results in very sluggish diffusion in these high entropy alloys, which in turn hinders rapid grain-growth, as often observed in most single-phase HEAs.

Figures 4(a,b) shows atom-probe tomographic (APT) reconstructions and respective data analysis results from the Al_{01}CoCrFeNi and $Al_{0.3}$CoCrFeNi HEAs, respectively, after these were subjected to annealing at 1150°C/60 min and subsequently water-quenched. The samples were lifted out from the regions close to (2–3 μm away) grain boundaries. All the atoms (ions) are displayed (different colors) in both reconstructions. While the raw atomic (ionic) maps look homogeneous in both cases, it should be noted that nanometer-scale short-range ordering/clustering tendencies cannot be statistically analyzed simply based on such pictorial depictions of the atomic-maps. A more statistical analysis of the randomness of the atomic distribution within such datasets involves dividing the dataset into bins of constant size (fixed number of atoms) and subsequently plotting a frequency-distribution plot of a number of bins versus the composition of the bin. If such a frequency-distribution plot exhibits a binomial distribution, then it

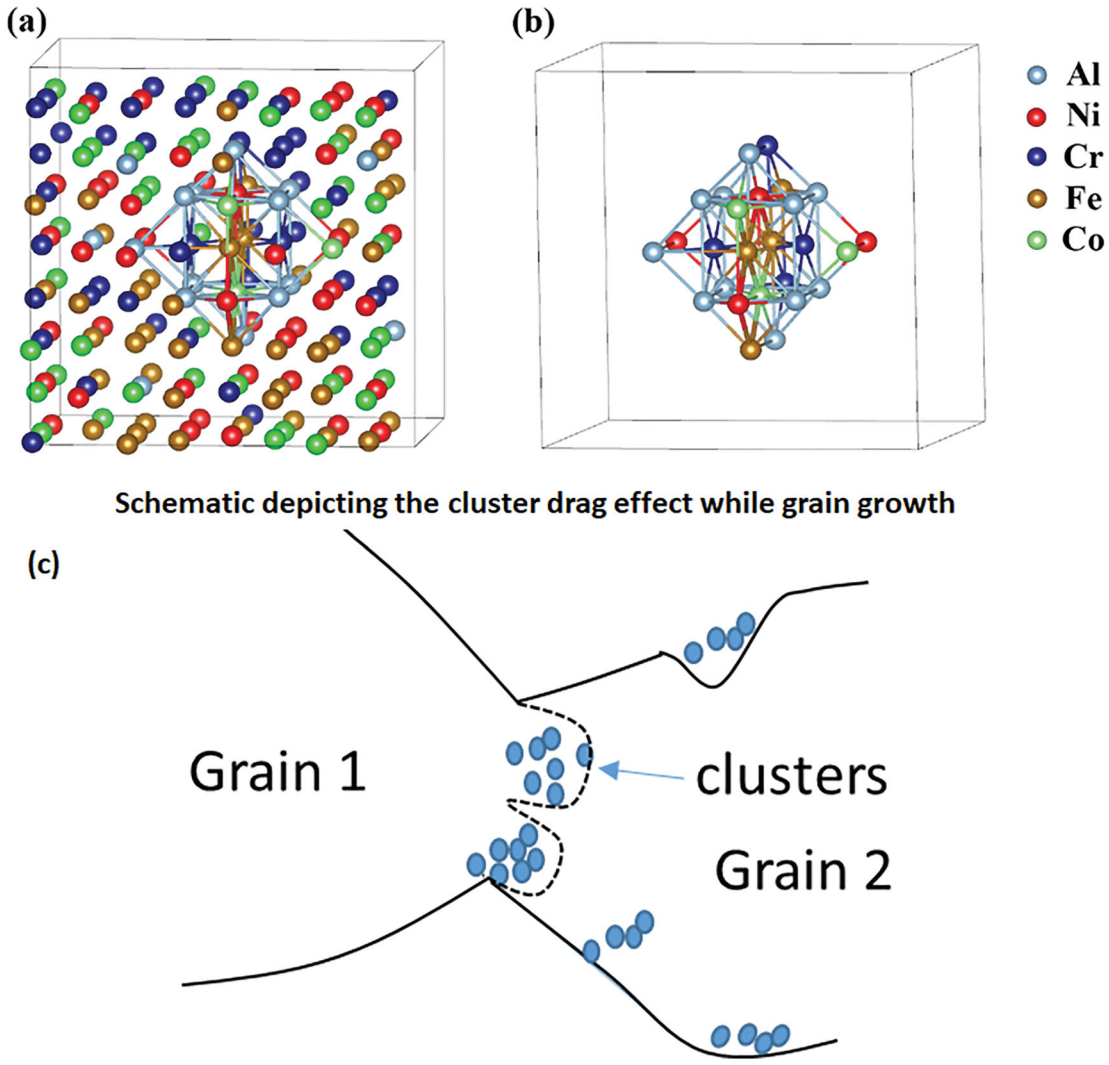

Figure 5. (a) The 192 atoms relaxed fcc supercell of $Al_{0.3}CoCrFeNi$ alloys with the cluster-domain demarked within it. (b) The cluster-domain of 26 atoms (10 Al, 4 of each other element) which corresponding to 38 at.% Al and 15 at.% of each other element. (b) A schematic showing the possible cluster-drag effect while the grain-growth.

represents a random distribution of the atoms within the analyzed volume [21–23–24]. The second set of figures in Figure 4(a,b), respectively, show the volumes employed for cluster analysis from the APT reconstructions of the $Al_{0.1}CoCrFeNi$ and $Al_{0.3}CoCrFeNi$ HEAs. The third set of figures (the extreme right set in Figure 4(a,b)) show the experimental frequency-distribution plot for Al atoms, as well as the simulated perfect binomial plot (representing random-distribution) for each alloy. While the experimental plot for the $Al_{0.1}CoCrFeNi$ HEA is in excellent agreement with the simulated binomial plot, indicating a true random distribution of the Al atoms, there is a significant difference in between the experimental and simulated plots for Al in case of the $Al_{0.3}CoCrFeNi$ HEA. Therefore, it can be concluded that in case of the $Al_{0.3}CoCrFeNi$ HEA, the Al atoms are not randomly distributed. Subsequently, a cluster-search algorithm was applied to the $Al_{0.3}CoCrFeNi$ dataset. The details of this technique can be found in the literature [17,23], and the step-by-step procedure is described in the IVAS™ 3.6.8 manual. After optimizing the parameters d_{max} and N_{min}, the actual cluster analysis was performed [23]. The d_{max} was 0.84 nm, and N_{min} was 33 ions. The number of clusters detected in the selected volume was 30, and cluster density was 8.33×10^{-4} nm^3/nm^3, average volume of clusters was 88 nm^3, average-diameter was 5.2 nm, and average-composition was 39Al-15Cr-14Fe-16Ni-16Co (at%). A visualization of these clusters in the $Al_{0.3}CoCrFeNi$ HEA is shown as an inset in the lower central part of Figure 4(b). The authors repeated the APT-experiments on two different generations on atom-probes 3000X HR and 5000XS. The results from

both instruments compared well. The details of results from 5000XS are provided as the supplementary information (Figure S5).

In order to provide more support on the experimentally observed clustering tendency of Al in Al_xCoCrFeNi (HEA) alloy, a series of DFT calculations were performed. Our simulation methodology involves building an *fcc* supercell where all elements are randomly distributed and then constructing a hemisphere cluster domain inside this supercell which resembles the APT experimental chemical analysis of the clustering, which has approx. 38 at.% Al, and 14 at.% of each other element. There is energy scatter associated with various distributions of the elements within the supercell so, different random configurations of supercell were created with different hemisphere inside while maintaining the chemical concentration of the elements within the domain. The average energy of these configuration were calculated. The relaxed *fcc* supercell with the hemisphere domain cluster is illustrated in Figure 5(a), in addition to the hemisphere cluster illustrated in Figure 5(b).

Two supercells with 192 atoms have been used, one with fully random distribution of all elements and another one also with random distribution of the elements but with a constructed cluster inside it. Twenty different random configurations have been utilized to calculate the average ground state energies of these two supercells with full relaxation of ionic positions and cell volume and shape. These calculations showed that the system that contains cluster has an average of 30 meV lower ground-state energy than the system without a cluster. This confirms the clustering tendency of Al in this alloy, which agrees with APT analysis results.

Additionally, another experiment was carried out to investigate the tendency to form Al-rich clusters in case of the $Al_{0.3}$CoCrFeNi alloy. Expediting and accentuating the formation of this short-range domain tendency is done by mechanically cold rolling this alloy followed by isothermal annealing at a lower temperature of 620°C for 1 h. The underlying rationale was that the cold-work will enhance the diffusion process while the lower annealing temperature will thermodynamically enhance the tendency to form Al-rich domains, due to the lower entropy contributions coupled with a stronger influence of the negative enthalpy of mixing of Al with the other constituent elements. The results of this cold worked and annealed samples are shown in Supplementary Figure S6. The TEM diffraction patterns, recorded from the [011] and [001] *fcc* zones, confirm the presence of a single *fcc* phase. However, the APT results from the same sample captured the strong tendency to form Al-rich domains, as shown in the APT reconstructions, with the Al atoms colored in yellow (Figure S6, bottom).

Summary

Grain-growth at three different temperatures for three *fcc*-based HEAs, $Al_{0.1}$CoCrFeNi, $Al_{0.2}$CoCrFeNi, and $Al_{0.3}$CoCrFeNi, exhibits a classical power law behavior ($n = 3$ exponent), with experimentally determined apparent activation-energies of 179, 321 and 486 kJ/mol, respectively. The power law exponent of 3 indicates that the grain-growth mechanism is largely controlled by the solute drag effect in addition to the interfacial tension at grain boundaries. Cluster analysis via APT clearly shows clustering/agglomeration of Al atoms in case of the $Al_{0.3}$CoCrFeNi HEA, while it is not observed in case of the $Al_{0.1}$CoCrFeNi HEA, Furthermore, DFT calculations confirm this tendency of Al in the $Al_{0.3}$CoCrFeNi alloy, indicating that the extremely large value of activation-energy (486 kJ/mol) in this alloy, is most likely due to a cluster-drag mechanism, which drastically slows down the grain-growth kinetic. The neutron-diffraction experiments of Ma et al. [2] also experimentally showed the presence of Al-rich domains in *fcc*-based single-phase an Al-Co-Cr-Fe-Ni based HEA alloy, which further establish the propensity of formation of nano-domains in these concentrated solid solutions. Figure 5(c) schematically illustrates the cluster-drag phenomenon wherein clusters of atoms (showing in blue color) hinder the motion of the adjacent grain boundary. The sluggish grain-growth kinetics arises because grain-boundary motion requires a concurrent migration of these domains/clusters. Nano-clustering in single-phase HEAs can have a much broader impact. Previous reports have shown that the strengthening coefficient (k) in the Hall–Petch equation increased from 371 MPa.$\mu m^{0.5}$ [25] to 824 MPa.$\mu m^{0.5}$ [26] on increasing the Al content in the *fcc* solid solution from $x = 0.1$ to 0.3 in the AlxCoCrFeNi alloy system. Therefore, these nano-clusters can potentially influence the lattice friction (or Pierels-Nabarro stress), dislocation-motion, amenability for deformation-twinning, Hall-Petch coefficients for hardness and yield strength, etc., in these HEAs, which can in turn affect the mechanical properties of these alloys. Interestingly, another recent paper by the authors on the $Al_{0.3}$CoCrFeNi alloy clearly shows the influence of more well-developed nano-clusters on extraordinary yield strengths in this alloy [18]. However, a fundamental understanding of the role of these nano-clusters on the deformation behavior and mechanical properties of these HEAs requires further detailed investigation.

Acknowlegdements

The authors acknowledge the Materials Research Facility (MRF) at the University of North Texas for use of microscopy

facilities, Talon2 and Stampede supercomputers at the University of North Texas and Texas Advanced Computing Center (TACC) at Austin for computational work.

Disclosure statement

No potential conflict of interest was reported by the authors.

Funding

The work was supported by cooperative agreement between the US Army Research Laboratory and the University of North Texas [grant number W911NF-16-2-0189], the US Air Force Office of Scientific Research [grant number FA9550-17-1-0395] and National Science Foundation (NSF) DEMREF program [grant number 1435611].

References

[1] Gludovatz B, Hohenwarter A, Catoor D, et al. A fracture-resistant high-entropy alloy for cryogenic applications. Science. 2014;345:1153–1158.
[2] Ma Y, Wang Q, Li C, et al. Chemical short-range orders and the induced structural transition in high-entropy alloys. Scr Materialia. 2018;144:64–68.
[3] Anderson MP, Srolovitz DJ, Grest GS, et al. Computer simulation of grain-growth—I. Kinetics. Acta Metall. 1984;32:783–791.
[4] Burke JE. Some factors affecting the rate of grain-growth in metals. AIME Trans. 1949;180:73–91.
[5] Beck PA, Kremer JC, Demer LJ, et al. Grain growth in high-purity aluminum and in an aluminum-magnesium alloy. Trans Am Inst Min Metall Eng. 1948;175:372–400.
[6] Rollett A, Humphreys FJ, Rohrer GS, et al. Recrystallization and related annealing phenomena. Kidlington (Oxford, UK): Elsevier; 2004.
[7] Burke JE, Shiau YG. The effect of mechanical deformation on grain-growth in alpha brass. AIME Trans. 1948;175:141–154.
[8] Grey EA, Higgins GT. Solute limited grain boundary migration: a rationalisation of grain-growth. Acta Metall. 1973;21:309–321.
[9] Grey EA, Higgins GT. A velocity independent drag during grain-boundary migration. Scr Metall. 1972;6:253–258.
[10] Bolling GF, Winegard WC. Some effects of impurities on grain-growth in zone-refined lead. Acta Metall. 1958;6:288–292.
[11] Bolling GF, Winegard WC. Grain-growth in zone-refined lead. Acta Metall. 1958;6:283–287.
[12] Lücke K, Detert K. A quantitative theory of grain-boundary motion and recrystallization in metals in the presence of impurities. Acta Metall. 1957;5:628.
[13] Cahn JW. The impurity-drag effect in grain boundary motion. Acta Metall. 1962;10:789.
[14] Lücke K, Stüwe HP. Recrystallization. In: Himmel L, editor. Recovery and recrystallization of metals. New York: Interscience; 1963. p. 171.
[15] Smith CS. Grains, phases, and interfaces: an introduction of microstructure. Trans. Am. Inst. Min. metall. Engrs. 1948;175:15.
[16] Gottstein G, Shvindlerman LS. Theory of grain boundary motion in the presence of mobile particles. Acta Metall Mater. 1993;41:3267–3275.
[17] Miller MK. Atom-probe tomography: the local electrode atom-probe. Boston (MA, USA): Springer; 2014. p. 320.
[18] Gwalani B, Gorsse S, Choudhuri D, et al. Tensile yield strength of a single bulk Al0.3CoCrFeNi high entropy alloy can be tuned from 160 MPa to 1800 MPa. Scr Materialia. 2019;162:18–23.
[19] Wu D, Zhang J, Huang JC, et al. Grain-boundary strengthening in nanocrystalline chromium and the Hall–petch coefficient of body-centered cubic metals. Scr Materialia. 2013;68:118–121.
[20] Liu WH, Wu Y, He JY, et al. Grain-growth and the Hall–Petch relationship in a high-entropy FeCrNiCoMn alloy. Scr Materialia. 2013;68:526–529.
[21] Juan C-C, Tsai M-H, Tsai C-W, et al. Simultaneously increasing the strength and ductility of a refractory high-entropy alloy via grain-refining. Mater Lett. 2016;184:200–203.
[22] Thompson K, Lawrence D, Larson DJ, et al. In situ site-specific specimen preparation for atom-probe tomography. Ultramicroscopy. 2007;107:131–139.
[23] Moody MP, Stephenson LT, Ceguerra AV, et al. Quantitative binomial distribution analyses of nanoscale like-solute atom clustering and segregation in atom probe tomography data. Microscopy research and technique. 2008;71:542–550.
[24] Hyde JM, Marquis EA, Wilford KB, et al. A sensitivity analysis of the maximum separation method for the characterisation of solute clusters. Ultramicroscopy. 2011;111:440–447.
[25] Kumar N, Komarasamy M, Nelaturu P, et al. Friction stir processing of a high entropy alloy $Al_{0.1}$CoCrFeNi JOM. 2015;67.5:1007–1013.
[26] Gwalani B, Soni V, Lee M, et al. Optimizing the coupled effects of Hall-Petch and precipitation strengthening in a $Al_{0.3}$CoCrFeNi high entropy alloy. Mater Des. 2017;121:254–260.